Shape optimisation of electro-mechanical ice protection systems

Valerian Palanque, Marc Budinger, Valerie Pommier-Budinger, Lokman Bennani

Shape optimisation of electro-mechanical ice protection systems

Valerian Palanque[1,4], Marc Budinger[2], Valerie Pommier-Budinger[3], Lokman Bennani[4]
1: ISAE-SUPAERO, ONERA/DMPE, University of Toulouse, F-31055 Toulouse - France, valerian.palanque@isae-supaero.fr
2: Institut Clément Ader (ICA), Université de Toulouse, INSA, ISA, marc.budinger@insa-tlse.fr
3: ISAE SUPAERO, Université de Toulouse, France, valerie.budinger@isae-supaero.fr
4: ONERA/DMPE, University of Toulouse, F-31055 Toulouse - France, lokman.bennani@onera.fr

Abstract
The ice protection system (IPS) is one of the major consumers among the non-propulsive systems of an aircraft. In the trend of the electrification of the aircraft systems to minimize air transport environmental impact, this article focuses on electromechanical IPS which could be a low power alternative to electro-thermal ice protection systems. The principle of resonant IPS is to deform the structure to create stresses in the ice greater than those required to remove the ice accumulated on the structure. Electromechanical IPS have been the subject of numerous studies and the mechanical mechanisms for ice fracture initiation and propagation are now better known. Ways of improving these systems have also been identified. Hence, this article proposes a methodology based on substrate shape optimization to improve the performances of such systems by increasing fracture propagation while minimizing the stress in the structure to avoid mechanical failure. This preliminary study shows that an increase in the protected area (up to 250%) is possible.
Experiments are conducted to confirm the computations. The final paper will include these experimental results.

Introduction

Icing occurs when an aircraft flies through clouds in which supercooled droplets are suspended in an atmosphere with an ambient air temperature below the freezing point. The droplets impinge on the aircraft surfaces and freeze, leading to ice accretion. The resulting change in the aircraft geometry can alter wing aerodynamic characteristics (loss of lift, increase in drag) or even damage the engine by ice ingestion. To overcome this issues, most aircrafts are now equipped with IPS. Even if most commercial aircraft IPS are non-electrical systems, electrical technologies are gradually getting more interest. Regarding electrical ice protection systems (IPS), electro-thermal and electro-expulse technologies are already implemented on aircraft, but studies are currently in progress to propose new solutions that consume less energy or have less bulky power supplies. This article focuses on electro-mechanical de-icing systems which are a subject of growing interest [1,2,3,4]. The principle of a mechanical ice protection system is to deform the structure to create stresses in the ice greater than those required to initiate and propagate fractures to remove the ice accumulated on the structure.
Thanks to the studies already achieved, the challenges to increase the Technology Readiness Level of electro-mechanical systems are now better identified:

- Develop a system efficient for any kind of ice (rime, glaze, mixed),
- Develop a control strategy which detects the ice thickness,
- Minimize the consumption and maximise the protected surface,
- Avoid mechanical failure of the protected structure and of the actuation system.

This article focuses on the two last challenges and proposes a methodology based on shape optimization to improve the performances of electro-mechanical systems by increasing fracture propagation while minimizing the stress in the structure, and consequently to the actuation system.

This article focuses mainly on mechanical considerations in order to improve the system. However, this is an unavoidable step in the development and the design of the electromechanical actuation system. The objective of this article is to show that an optimisation of the structure can help design an efficient electro-mechanical de-icing system that consumes less than current IPS.

Fracture mechanisms in mechanical IPS

This article focuses on electro-mechanical de-icing systems that use an actuation system creating a quasi-static deformation. For this configuration, the assumed fracture mechanism (Fig. 1) is a three-step mechanism:

- firstly, cohesive fractures are initiated due to tensile stress on the ice surface,
- secondly, right after the initiation of cohesive fractures at the top surface of the ice layer, the cohesive fractures propagate through the ice,
- thirdly, adhesive fractures propagate at the ice/substrate interface, starting from the base of the cohesive fractures previously created.

This mechanism has been established with regards to literature on fracture propagation and validated by experimental tests on a plate deformed in its middle (Fig.2).

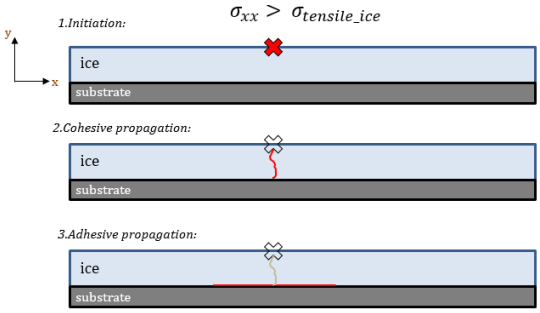

Fig. 1: Fracture mechanism in ice

Fig. 2: Observed cohesive and adhesive fractures

Fracture initiation and propagation in ice

The proposed computational method to study the initiation of fractures in ice consists in computing tensile stress in ice and shear stress at the ice/structure interface and to compare these values with respectively the cohesive strength in ice and the adhesive shear strength at the ice/structure interface (see Table 1). If the stresses are greater than the material strengths, it is assumed that fractures initiation is possible.

The computational method to study the propagation of cohesive and adhesive fractures is based on the classical Griffith energy balance approach [4]. While assuming the fracture path, using strain energy finite differences, this method allows studying the fracture behaviour: stable or unstable propagation. The strain energy release rates in ice (cohesive) and at the ice/structure interface (adhesive) are evaluated respectively by the formula:

$$G_{coh_{X\%}} = -\frac{1}{b}\left(\frac{\partial u}{\partial L_{f,coh}}\right)\Big|_{\frac{L_{f,coh}}{t}=X\%} \quad (1)$$

and

$$G_{adh_{X\%}} = -\frac{1}{b}\left(\frac{\partial u}{\partial L_{f,adh}}\right)\Big|_{\frac{L_{f,adh}}{l}=X\%} \quad (2)$$

with b the depth of the plate, u_i the stored elastic energy, and L_f the length of the fracture ($L_{f,coh_{X\%}}$ for cohesive fractures and $L_{f,adh_{X\%}}$ for adhesive fractures). $X\%$ represents the fracture length according to the ice thickness ($coh_{X\%}$) or to the plate length ($adh_{X\%}$).

Then $G_{coh_{X\%}}$ or $G_{adh_{X\%}}$ are then compared to the critical strain energy release rate, G_c (here assumed to have the same value in ice or at the ice / structure interface, see Table 1). Two situations can occur (Fig. 3). Either $G_{coh_{X\%}}$ or $G_{adh_{X\%}}$ are smaller than the critical value G_c and the propagation is said to be stable, which implies that energy input is required to pursue the propagation (to raise $G_{coh_{X\%}}$ or $G_{adh_{X\%}}$ to the G_c value), or the propagation is unstable and, fracture propagates instantaneously, which is a more favourable situation.

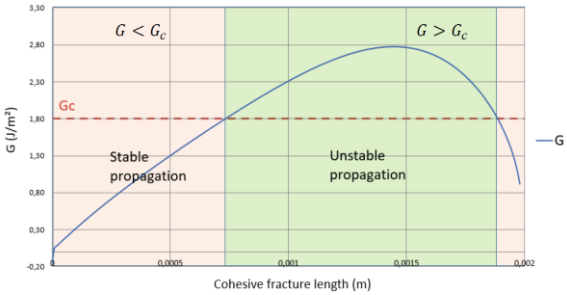

Fig. 3: Example of fracture propagation $G_{coh_{X\%}}$ through a 2mm-thick ice layer

Mechanical properties in ice and at the ice/structure interface	
Ice Cohesive strength	[0.6-3] MPa
Adhesive shear strength (ice/structure)	[0.2-1] MPa
Critical strain energy release rate, G_c(ice or ice/structure)	[0.5-1] J/m²

Table 1 – Strength and critical strain energy release rate [5,6]

Shape Optimisation problem

To get an efficient de-icing, delamination of ice over the entire structure is required, which means that adhesive fractures must propagate. From our experiments, adhesive fractures are the most difficult to obtain. Their propagation depends on the structure boundary conditions, the mechanical solicitation and on the shape of the structure.

The work here after presented aims at optimising the structure thickness to maximise the fracture

propagation while ensuring that the stress in the structure is acceptable. A key performance indicator (KPI) is defined to assess the result of the optimisation:

$$\mathrm{KPI} = \frac{\mathrm{G_{adh_{X\%}}}}{\sigma^2_{structure}} \qquad (3)$$

where $\sigma_{structure}$ is the Von Mises stress in the structure. The choice to select $\frac{\mathrm{G_{adh_{X\%}}}}{\sigma^2_{\mathrm{structure}}}$ and not $\frac{\mathrm{G_{adh_{X\%}}}}{\sigma_{\mathrm{structure}}}$ is guided by the idea of obtaining a cost function that depends only on the structure and not on the displacement of the external solicitation. As stress is proportional to displacement amplitude and the energy release rate is proportional to the square of displacement amplitude, the proposed KPI is thus the ratio between the energy release rate and the square of stress σ. Hence, this KPI enables to study the propagation capability of the structure regardless of the displacement amplitude while ensuring that its mechanical properties are not exceeded. In this way, shape optimisation can be performed to design the structure.
The actuation system will be designed in a second step with the objective to create the required displacement to reach the critical energy release rate G_c.

Optimisation of an electro-mechanical IPS
We consider here a narrow plate clamped on both opposite sides and subjected to a displacement in its center.

Fig. 4: Schematic view of the beam model

The stress and energy distribution will be optimized via the thickness of the substrate. This thickness distribution will notably influence the evolution of the bending moment.

$$M_{bending}(x) = F_A.x - M_A = -\frac{F.x}{2} + \frac{F.L}{8}.k \qquad (4)$$

Where x is the position along the beam and k is a factor expressing the moment at clamped (A) position. k is also an image of the position of the inflection point of the beam. For k between 0 and 1, the inflection point is moved toward the clamped boundary and therefor the tensile area of the beam and the delamination area are extended.

The design is performed through two consecutive steps in order to perform a multi-objective optimization:
- step 1: maximize the delamination area
  - by extending the theoretical delamination area: minimizing the factor k which has an impact on the bending moment;
  - by extending the practical delamination area: maximizing the $\mathrm{KPI} = \frac{\mathrm{G_{adh_{X\%}}}}{\sigma^2_{structure}}$ value.
- step 2: minimizing the mass
  by accepting a controlled loss on the de-icing performance of previously optimized solution.

Consequently, for step 1, the optimization problem is formulated as:

$$obj_1 = \min_{h \in [h_{min};h_{max}]} \frac{< k >}{\left(< \frac{G}{{\sigma_{max}}^2} . \frac{{\sigma_{adm}}^2}{G_c} >\right)} \qquad (4)$$

with $< x >$ meaning the mean value of the x vector and h being the optimized substrate thickness.

As $\frac{\mathrm{G_{adh_{X\%}}}}{\sigma^2_{structure}} > \frac{G_c}{\sigma^2_{adm}}$ being the fracture condition, for numerical purposes, the KPI can be normalized using the ratio $\frac{G_c}{\sigma^2_{adm}}$ with G_c the critical energy release rate of the material and σ_{adm} the mechanical strength of the structure.

The optimisation is performed on half a beam divided in N segments, numbered starting from the clamped side of the beam.

The first optimisation is performed under two numerical constraints:

$$C_1 = \frac{\sigma_{ice_{max}}}{\sigma_{max}} > \frac{\sigma_{admice}}{\sigma_{adm}} \qquad (6)$$

$$C_2 = \sigma_{ice}[i+1] > \sigma_{ice}[i].\varepsilon, \mathrm{i{=}0..N\text{-}1} \qquad (7)$$

with $\sigma_{ice_{max}}$ the maximum normal stress in the ice, σ_{max} the maximum stress in the substrate and $\frac{\sigma_{admice}}{\sigma_{adm}}$ the ratio between the tensile strength of the ice and the tensile strength of the substrate.

C_1 ensures that there is no risk of failure in the structure before initiating the crack in the ice.
C_2 is defined to ensure a minimum slope ε in the variation of the stress in the ice to ensure that the fracture mechanism occurs as defined in Fig. 1, with the initiation of the cohesive crack occurs in the middle of the beam and–without any subsequent cohesive crack after the first fracture initiation.

For the second step, the optimization problem is formulated as:

$$obj_2 = \min_{h \in [h_{min};h_{max}]} \{Mass + < k >\} \qquad (8)$$

k is the previously defined parameter to help convergence of the second optimization in a direction that follows the first optimization path.

A constraint function is added:

$$C_3 = \left(1 + Coef_{optim}\right).obj_{1\ step1} > obj_{1\ step2} \qquad (9)$$

where $obj_{1\ step1}$ is the value of the objective computed in the first optimization which is fixed for the second set and $obj_{1\ step2}$is the scalar value of the same objective computed in the second step. $Coef_{optim}$ is a numerical parameter used to define the loss allowed in delamination performance compared to the first optimization step.

Validation on a simplified case

The proposed methodology is applied to an aluminium alloy plate. The plate dimensions are 130x40x1.5 mm³. Fig. 5. shows the shape of the optimized substrate and Fig. 6 the 3D CAD modelling of the optimised sample.. The thickness is increased at the centre of the beam to smooth the normal stress which is maximum in the middle. In order to help the structure withstanding the load, thickness is also increased on the clamped sides so that the maximum stress in the structure stays in the middle of the beam.

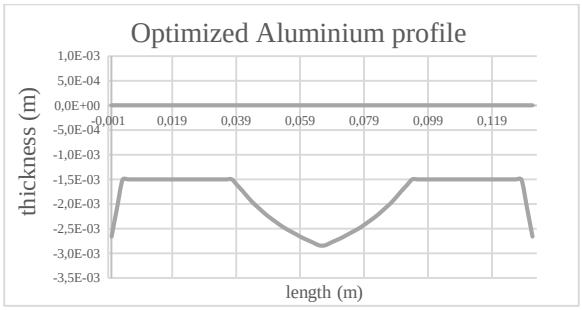

Fig. 5: Optimized thickness versus the beam position

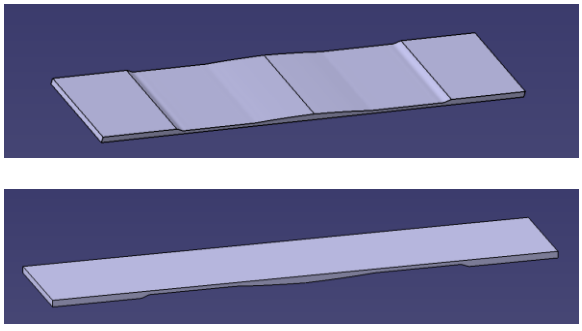

Fig. 6: 3D modelling of the optimised sample

Fig. 7 shows that this optimised profile makes it possible to increase the KPI value and shows the fracture lengths for non-optimized and optimized beam. Two thresh-old are drawn for the minimum and the maximum G_c value from Table 1. Theses limits show that even with the inherent uncertainty of the ice mechanical properties, the optimisation increases the system performances. For the regular beam, the propagation length lies between 18% and 28% of the substrate area, however, optimization shows that this length can be increased between 43% and 50%.

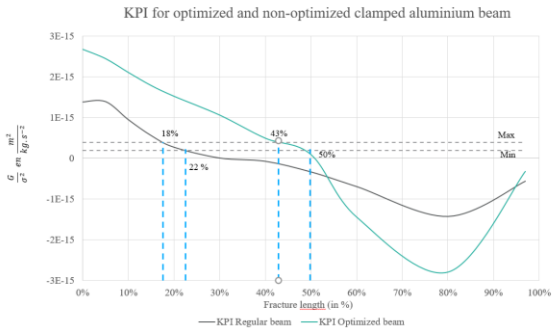

Fig. 7: key performance indicator versus the fracture length (half a beam represented)

Energetic potential of electro-mechanical de-icing systems compared to electro-thermal de-icing systems

Electro-thermal de-icing involves melting a few tenths of mm of the layer of ice at the interface with the leading edge, which gives a surface energy of about 10^5 J/m².

Mechanical deicing mainly involves fracturing the ice/substrate interface. The minimum energy required is expressed by the critical energy release rate (Griffith criterion) of value 1 J/m^2. The energy release rate G is proportional to the strain energy of the structure U. Figure 7 shows the $\frac{G}{U}$ ratio for our study case. This ratio is worth 5.53e-01 m^{-2} for the maximal delamination of 50%, which corresponds to a delaminated surface of 26.0 cm². The required surface energy is thus 695 J/m².

Therefore, a consumption ratio of 144 between electro thermal and electromechanical deicing can be considered for the considered case.

Of course, this ratio is theoretical and may be adjusted with the differences due to the type of ice, the presence of coating, the efficiency of the actuation system, etc. The difference of activation time will affect the power consumption ratio.

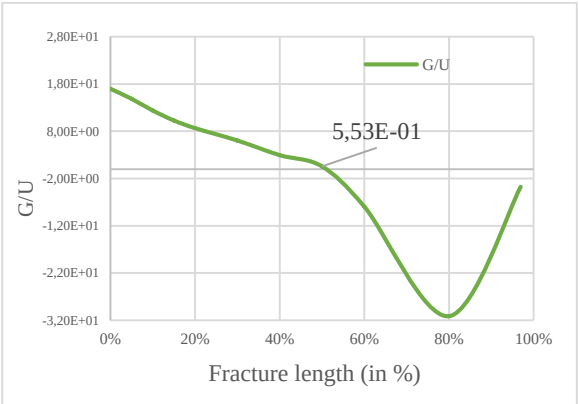

Fig. 8: Normalized energy release rate versus the fracture length (half a beam represented)

Conclusions

Low frequency electro-mechanical de-icing are expected to have relatively low electrical requirements in comparison to electro-thermal de-icing systems. However, the fracture propagation and thus the protected area can be limited. This article shows how shape optimization can be effective to beat off this limit. The protected area can be extended to 50%, which can be sufficient on some cases (e.g. a leading edge is not completely covered by ice). In an energy consumption way, the consumption seems reducible by 144. This shows that electro-mechanical technologies could be a relevant alternative for aircrafts ice protection.

References

1. Palacios, J., Smith, E., Rose, J., & Royer, R. (2011). Ultrasonic de-icing of wind-tunnel impact icing. Journal of Aircraft, 48(3), 1020-1027, DOI: 10.2514/1.C031201
2. Villeneuve, E., Volat, C., Ghinet, S. Numerical and Experimental Investigation of the Design of a Piezoelectric De-Icing System for Small Rotorcraft Part 1/3: Development of a Flat Plate Numerical Model with Experimental Validation. Aerospace 2020, 7, 62. DOI: 10.3390/aerospace7050062
3. Pommier-Budinger, V., Budinger, M., Rouset, P., Dezitter, F., Huet, F., Wetterwald, M., & Bonaccurso, E. (2018). Electromechanical Resonant Ice Protection Systems: Initiation of Fractures with Piezoelectric Actuators. AIAA Journal, 56(11), 4400-4411. DOI: 10.2514/1.J056662
4. Budinger, M., Pommier-Budinger, V., Bennani, L., Rouset, P., Bonaccurso, E., & Dezitter, F. (2018). Electromechanical Resonant Ice Protection Systems: Analysis of Fracture Propagation Mechanisms. AIAA Journal, 56(11), 4412-4422. DOI: 10.2514/1.J056663
5. Bennani, L. (2014). Two dimensional modelling of electrothermal ice protection systems (Doctoral dissertation).
6. Guerin, F., Laforte, C., Farinas, M. I., & Perron, J. (2016). Analytical model based on experimental data of centrifuge ice adhesion tests with different substrates. Cold Regions Science and Technology, 121, 93-99. DOI: 10.1016/j.coldregions.2015.10.011